



UNIVERSITÀ
DEGLI STUDI
FIRENZE

FLORE

Repository istituzionale dell'Università degli Studi di Firenze

Additional value of gadoxetic acid-DTPA-enhanced hepatobiliary phase MR imaging in the diagnosis of early-stage hepatocellular

Questa è la Versione finale referata (Post print/Accepted manuscript) della seguente pubblicazione:

Original Citation:

Additional value of gadoxetic acid-DTPA-enhanced hepatobiliary phase MR imaging in the diagnosis of early-stage hepatocellular carcinoma: comparison with dynamic triple-phase multidetector CT imaging / Haradome H; Grazioli L; Tinti R; Morone M; Motosugi U; Sano K; Ichikawa T; Kwee TC; Colagrande S.. - In: JOURNAL OF MAGNETIC RESONANCE IMAGING. - ISSN 1053-1807. - ELETTRONICO. - 34:(2011), pp. 69-78.

Availability:

The webpage <https://hdl.handle.net/2158/508485> of the repository was last updated on

Published version:

DOI: 10.1002/jmri.22588

Terms of use:

Open Access

La pubblicazione è resa disponibile sotto le norme e i termini della licenza di deposito, secondo quanto stabilito dalla Policy per l'accesso aperto dell'Università degli Studi di Firenze (<https://www.sba.unifi.it/upload/policy-oa-2016-1.pdf>)

Publisher copyright claim:

La data sopra indicata si riferisce all'ultimo aggiornamento della scheda del Repository FloRe - The above-mentioned date refers to the last update of the record in the Institutional Repository FloRe

(Article begins on next page)

Original Research

Additional Value of Gadoxetic Acid-DTPA-Enhanced Hepatobiliary Phase MR Imaging in the Diagnosis of Early-Stage Hepatocellular Carcinoma: Comparison With Dynamic Triple-Phase Multidetector CT Imaging

Hiroki Haradome, MD, PhD,^{1,2*} Luigi Grazioli, MD, PhD,¹ Rita Tinti, MD,¹ Mario Morone, MD,¹ Utaroh Motosugi, MD, PhD,³ Katsuhiko Sano, MD,³ Tomoaki Ichikawa, MD, PhD,³ Thomas C. Kwee, MD, PhD,⁴ and Stefano Colagrande, MD, PhD⁵

Purpose: To assess the value of hepatobiliary phase gadoxetic acid (EOB)-enhanced magnetic resonance imaging (MRI) for the diagnosis of early stage hepatocellular carcinoma (HCC) (<3 cm) compared to triple-phase dynamic multidetector computed tomography (MDCT).

Materials and Methods: In all, 52 patients with 60 pathologically proven HCCs underwent both EOB-enhanced MRI and triple-phase dynamic MDCT. Two radiologists independently and blindly reviewed three image sets: 1) MDCT, 2) dynamic MRI (unenhanced and EOB-enhanced dynamic MR images), and 3) combined MRI (dynamic MRI + hepatobiliary phase images) using a five-point rating scale on a lesion-by-lesion basis. Receiver operating characteristics (ROC) analysis was performed, and sensitivity and specificity were calculated.

Results: The area under the ROC curve (Az) of dynamic MRI was equivalent to that of MDCT for both readers. For both readers, Az and sensitivity of combined MRI for smaller lesions (<1.5 cm) were significantly higher than that of dynamic MRI and MDCT ($P < 0.0166$). The majority of false-negative nodules on dynamic MRI or MDCT (75% and 62%, respectively) were due to a lack of identified washout findings.

Conclusion: Hepatobiliary phase images can increase the value of EOB-enhanced MRI in the diagnosis of early

stage HCC. The sensitivity and accuracy were significantly superior to MDCT for the diagnosis of lesions less than 1.5 cm.

Key Words: MRI; gadoxetic acid disodium; hepatocellular carcinoma; MDCT; liver

J. Magn. Reson. Imaging 2011; 34:69–78.

© 2011 Wiley-Liss, Inc.

HEPATOCELLULAR CARCINOMA (HCC) is the sixth most common cancer worldwide and the third most frequent cause of cancer death (1). HCC is the main cause of death among cirrhotic patients and the incidence of HCC is predicted to increase in the next two decades (2). The diagnosis of early stage HCC, which can be curable by partial hepatic resection, liver transplantation, or locoregional therapies, is crucial during the follow-up of high-risk patients. For instance, early stage of the Barcelona-Clinic-Liver-Cancer (BCLC) staging system or the Milan criteria include patients with fewer than three nodules less than 3 cm in size or a solitary lesion less than 5 cm (3,4). Thus, the earlier detection of HCC (at least less than 3 cm) by each imaging modality is a keystone in the risk group patients. Both multidetector computed tomography (MDCT) and magnetic resonance imaging (MRI) play an important role in the accurate staging of HCC in cirrhotic patients (5–7). Among a variety of commercially available liver MR contrast agents, the newly introduced contrast agent gadoxetic acid (EOB) has theoretical advantages over extracellular agents. Similar to extracellular contrast agents, EOB allows for dynamic perfusion imaging to evaluate tumor vascularity. However, since it is also taken up by hepatocytes, it also allows for liver-specific imaging (hepatobiliary phase images) (8). The higher T1 relaxivity of EOB in human blood due to its weak protein binding

¹Department of Radiology, University of Brescia, Spedali Civili di Brescia, Italy.

²Department of Radiology, Kyorin University School of Medicine, Tokyo, Japan.

³Department of Radiology, University of Yamanashi, Japan.

⁴Department of Radiology, University Medical Center Utrecht, Utrecht, Netherlands.

⁵Department of Radiology, University of Florence, Italy.

*Address reprint requests to: H.H., Piazzale Spedali Civili 1, 25123, Brescia (BS), Italy. E-mail: karate.b@gmail.com

Received December 24, 2010; Accepted March 7, 2011.

DOI 10.1002/jmri.22588

View this article online at wileyonlinelibrary.com.

(10%) could contribute to stronger enhancement on arterial phase images. The specific uptake of EOB in functioning hepatocytes on hepatobiliary phase images is another factor that may increase lesion-to-liver contrast and the detectability of small lesions (9,10). As the American Association for the Study of Liver Diseases (AASLD) and the European Association for the Study of the Liver (EASL) indicate (11,12), the diagnosis of HCC using extracellular agents is based mainly on assessment of tumor vascularity: hyperenhancement in the arterial phase followed by rapid washout in portal venous or equilibrium phase. Although these criteria have been established for the diagnosis of HCC, they have some limitations because the vascularity may vary depending on the histological grading of HCC, whereas technical aspects (hardware, injection methods, etc.) could influence sensitivity of the arterial enhancement. EOB is not only an excellent extracellular agent providing information on tumor vascularity, but it also has a hepatocyte-specific property, which could aid in the diagnosis of HCC. Recent reports indicated similar or superior diagnostic performance of EOB-enhanced MRI compared to dynamic MDCT (13–18) and hepatobiliary phase images provided modest improvement in the diagnosis of HCC (16). However, to the best of our knowledge, there have been some comparative studies between MDCT imaging and gadolinium (Gd)-EOB-DTPA-enhanced MRI for the diagnosis of HCC and few studies assessing the usefulness of hepatobiliary phase images adding Gd-EOB-DTPA-enhanced MRI for comparison with MDCT imaging (18). The purpose of this study was therefore to evaluate the added value of hepatobiliary phase EOB-enhanced MRI for the diagnosis of early stage HCC compared to triple-phase dynamic MDCT.

MATERIALS AND METHODS

This study complied with the principles of the Declaration of Helsinki and subsequent amendments (19). Our Institutional Review Board approved this study (EOB has been approved for clinical use since November 2006 in Italy and the indication was according to the label) and written informed consent was waived. All data and information derived from and pertaining to the study were under the exclusive control of the investigating radiologists.

Patient Population

From January 2008 to July 2009 we retrospectively reviewed our hospital reporting database of both abdominal CT and MRI examinations in patients with suspected HCC. We found 176 consecutive patients suspected of having HCC. Among these patients, 46 patients were excluded from the study because of a lack of satisfactory confirmation (ie, if both pathological proof and sufficient follow-up examinations were not available). Fifty-five patients were considered ineligible for the study because of 1) a long interval between MDCT and MRI (more than 21 days) ($n = 26$);

Table 1
Clinical information of the 75 patients and characteristics of 60 HCC lesions

Age range (mean age)	42–67 years (54.7 years)
Sex (M/F)	60/15
Diagnosis of the lesions ($n = 86$)	60 HCC, 10 hemangioma, 16 A-P shunt
Characteristics of 60 HCCs (52 pts)	
a. Mean size \pm SD	17.4 \pm 6.53 mm (12 HCCs \leq 10 mm)
b. Location	39 in right lobe 21 in left lobe
c. Histopathology	10 well-differentiated 28 moderately-differentiated 22 poorly-differentiated
Background liver ($n = 75$ pts)	54 LC, 4 CH, 3 steatosis, 4 normal
Cause of LC	23 HCV 14 HBV 4 HCV+HBV 10 Alcohol 3 cryptogenic
Child-Pugh classification	48 Child A 5 Child B 1 Child C

Note: HCC: Hepatocellular carcinoma; LC: Liver cirrhosis; CH: Chronic hepatitis.

HBV: Hepatitis B virus; HCV: Hepatitis C virus.

2) the presence of more than 10 HCC lesions ($n = 18$); or 3) inadequate MDCT examination ($n = 6$) (extravasation of contrast agent or equipment failure) or MRI examination ($n = 5$) (nondiagnostic image quality due to severe motion artifacts).

Finally, 75 patients (60 men and 15 women; age range 42–67 years; mean age 54.7 years) with a total of 86 nodules were enrolled in this study. Clinical information of the patients and characteristics of the HCC lesions are summarized in Table 1. Among the 86 nodules, 60 nodules were HCCs, 10 nodules were hemangiomas, and the remaining 16 nodules were arteriportal (A-P) shunts. In all, 38 patients had only HCC, 14 had HCC accompanied with hemangioma or A-P shunt, and seven had only hemangioma or A-P shunt. The diagnosis of all 60 HCC nodules was achieved based on pathologic specimens: surgical resection ($n = 19$) or fine needle biopsy ($n = 41$). Out of 60 pathologically proven HCCs, 10 were well-differentiated, 28 were moderately differentiated, and 22 were poorly differentiated. The 36 benign lesions were confirmed by the fact that these lesions did not show any interval change in size at follow-up CT or MRI for more than 6 months and/or typical imaging findings at multimodality examinations, including contrast-enhanced ultrasound (US) and follow-up studies. The mean diameter \pm standard deviation of HCC was 17.4 \pm 6.53 mm (range, 5–28 mm), and 12 (20%) HCCs had a diameter of 10 mm or less, as measured on those images on which the lesions were most clearly visualized (eg, arterial or hepatobiliary phases) on reading sessions. The 21 HCCs were located in the left lobe (S1–4) and the remaining 39 HCCs were

located in the right lobe (S5–8). Twenty-three patients had hepatitis C virus (HCV)-induced liver cirrhosis, 18 patients had liver cirrhosis ($n = 14$) or chronic hepatitis ($n = 4$) associated with hepatitis B virus (HBV), four patients had HCV and HBV-induced liver cirrhosis, 10 patients had alcohol-related cirrhosis (four combined with HCV and two combined with HBV), and three patients had cryptogenic liver cirrhosis. Seventeen patients had a noncirrhotic liver (14 normal livers and three steatotic livers). The severity of liver cirrhosis was based on the Child-Pugh classification: 48 patients were classified as Child class A, 5 patients as Child class B, and the remaining patient as Child class C. The time interval between MDCT and MRI ranged between 3 and 20 days (mean, 9.3 days).

MDCT Examination

CT examinations were conducted using an MDCT scanner (Sensation 16, Siemens Medical Systems, Erlangen, Germany) with 16 detector rows. The images were obtained in the craniocaudal direction with 0.75×16 beam collimation. The scanning parameters were 120 kVp, 150 mAs, 5-mm slice thickness with a reconstruction interval of 3.0 mm, table speed of 24 mm (pitch 1.5:1), 0.5-second gantry rotation time, volumetric CT dose index of 10.7 mGy, and a single breath-hold helical acquisition of 7–9 seconds depending on the liver volume of each patient. All patients received intravenous nonionic contrast medium (Ultravist 370, Bayer Schering Pharma, Berlin, Germany) containing a high concentration of iodine (370 mg of iodine per kg). The volume of delivered contrast medium was determined according to the body weight of each patient (1.8 mL/kg of body weight). The contrast medium was warmed to decrease its viscosity and administered intravenously at 4 mL/sec with a mechanical power injector (Missouri, Ulrich, Ulm, Germany), followed by a 40-mL saline flush through a 20G catheter inserted into an antecubital vein. After precontrast imaging, CT imaging was performed during dominant hepatic arterial, portal venous, and late phases at 26–30 seconds (mean 28.4 sec), 70 seconds, and 180 seconds, respectively, after the administration of the contrast medium. The time-to-peak aortic enhancement was evaluated by an automatic bolus-tracking technique with automated scan-triggering software (CARE Bolus CT; Siemens Medical Systems) to determine the optimal scanning delay for the arterial phase in all patients. The single level monitoring low dose scanning (20 mAs) was initiated 5 seconds after contrast injection and arterial phase scanning was started automatically 15 seconds after the trigger threshold (increase of 120 HU) had been reached at the level of the suprarenal abdominal aorta.

MR Examination

MRI was performed with a 1.5-T scanner (Avanto, Siemens Medical Systems) equipped with an 18-channel system (maximum gradient strength of 45 mT/m,

peak slew rate of 200 mT/m/msec) and a 12-element phased-array surface body coil. All MR images were acquired in the transverse plane covering the upper abdomen during end-expiratory breath-hold or with respiratory triggering. Presaturation pulses were applied above and below the imaging volume to reduce flow artifacts from vessels. All MR images were acquired using mSENSE (reduction factor = 2) to reduce scanning time. Before administration of the contrast agent, dual-echo T1-weighted (T1W) gradient-echo (GRE) sequence (repetition time/echo times [TR/TEs], 131/2.6/5 out phase / in phase; flip angle, 70°; matrix size, 166×256 ; bandwidth, 260 Hz/pixel; field of view [FOV], 38–50 cm) with breath-hold and a 5-mm section thickness, respiratory triggered T2-weighted (T2W) turbo spin-echo (TSE) sequence (TR/TE, 1600/79; flip angle, 150°; matrix size, 166×256 ; bandwidth, 260 Hz/pixel; FOV, 38–50 cm), without fat suppression and a 5-mm section thickness were obtained. After these precontrast images, a T1W 3D GRE fat-saturated volumetric interpolated breath-hold examination sequence (VIBE; Siemens) (TR/TE 5.2/2.5; flip angle, 10°; matrix size, 166×320 ; bandwidth, 250 Hz/pixel; FOV, 38–50 cm; voxel size, 1.72 [read] $\times 1.19$ (phase) $\times 4.00$ mm [slice]) with a 4-mm section thickness was acquired before administration of the contrast agent and during the arterial phase at 25–37 seconds (mean delay time, 30.5 sec), during the portal venous phase at 70 seconds, during the equilibrium phase at 180 seconds, and during the hepatobiliary phase at 5 minutes, 10 minutes, 15 minutes, and 20 minutes, respectively. We also used the MR fluoroscopic bolus detection technique (CARE Bolus; Siemens) to adjust optimal scan delay timing for arterial phase imaging. In all patients, 0.025 mmol/kg body weight of EOB (Primovist, Bayer Schering Pharma) was administered at 1 mL/sec intravenously as recommended with a mechanical power injector (MedRad Spectris Solaris EP) through a 20G catheter inserted into an antecubital vein, followed by a 20-mL saline flush at the same injection rate (20). Between 5 minutes and 20 minutes after administration of the contrast medium, respiratory triggered T2W-TSE sequence with fat suppression and navigator triggered diffusion-weighted echo planar sequence (DWI) (TR/TE of 2000/71 msec; section thickness/gap, 6/1.2 mm; FOV, 32–45 cm; matrix size, 77×192 ; echo train length, 77; bandwidth, 628 Hz/pixel; spectral attenuated inversion recovery [SPAIR] fat suppression; number of excitations, 2; tridirectional motion probing gradients with b-values of 50, 400, and 800 s/mm²; image acquisition time, 4–5 minutes) were obtained.

Image Analysis

Two abdominal radiologists with 21 and 15 years of experience, respectively, in the interpretation of hepatic MR images independently, blindly, and randomly evaluated three imaging modalities: 1) triphase dynamic MDCT (arterial, portal, and equilibrium phases); 2) dynamic MRI: unenhanced (precontrast T1WI and T2WI) and EOB-enhanced dynamic images

(arterial, portal, and late phases); 3) combined MRI: dynamic + hepatobiliary phase images on a lesion-by-lesion basis. The readers were aware of the image phase and that all patients had cirrhosis and suspected HCC, but were unaware of the results of tumor histopathology, US findings, tumor marker levels (eg, AFP, PIVKA II), and the opinions of other readers. All images were assessed on a local picture archiving and communication system monitor (iSite Radiology, Philips Healthcare). The images were adjusted to an optimal window setting in each case and the readers evaluated them in the same conditions. To minimize recognition bias, reading sessions occurred at 3-week intervals. For objectivity and reproducibility, the readers were instructed to use the following criteria for supporting the diagnosis of HCC: i) intense arterial enhancement and hypoattenuation or hypointensity compared with surrounding liver parenchyma (wash-out) during portal venous or equilibrium/late phases; ii) peripheral rim enhancement during portal venous or equilibrium/late phases; and iii) intense arterial enhancement and hypointensity during hepatobiliary phase (12). Suggestive criteria for the diagnosis of HCC included a) moderate hyperintensity on T2WI or DWI; b) nodular arterial enhancement without washout during portal venous and equilibrium/late phases; c) nodular arterial enhancement and isointensity during the hepatobiliary phase; and d) lesions showing hyperintensity compared to surrounding liver parenchyma during the hepatobiliary phase and on T2WI or DWI. Meanwhile, the following criteria were used to diagnose benign lesions (hemangioma or A-P shunt): 1) peripheral nodular or global enhancement during arterial phase and prolonged enhancement during portal venous and/or equilibrium/late phases, and 2) wedged-shaped arterial enhancement located at the peripheral liver with/without early delineation of peripheral portal branches and isoattenuation or isointensity during portal venous, equilibrium/late, or hepatobiliary phases.

First, each reader recorded the size (defined as the maximum diameter), the segmental location according to the Couinaud classification, and the attenuation or intensity on precontrast images of each lesion. Then the readers recorded the attenuation or intensity compared to surrounding liver parenchyma of each lesion during arterial, portal venous, equilibrium/late, and hepatobiliary phases.

Finally, based on the above-mentioned criteria, each reader classified each lesion using the following five-point confidence scale: score 1, no HCC; score 2, probably no HCC; score 3, intermediate; score 4, probably HCC; score 5, definite HCC. In patients with multiple lesions, in addition to the descriptions of size and segmental location of the lesions, the readers drew arrows with numbers for all lesions that were evaluated, which were saved as digital images in the workstation to avoid a mismatch between lesions identified with MDCT, MRI, and the reference standard.

Statistical Analysis

Receiver operating characteristics (ROC) analysis was performed to evaluate the diagnostic performance of

Table 2

Az values of each set of images in the diagnosis of HCC for the two readers

	MDCT	Dynamic MRI	Combined MRI
All lesion (n = 60)			
Reader 1	0.921	0.925	0.961 [†]
Reader 2	0.917	0.935	0.967 [†]
Mean	0.919	0.930	0.964
Lesion <1.5 cm (n = 16)			
Reader 1	0.765	0.890	0.952*
Reader 2	0.765	0.858	0.952*
Mean	0.765	0.874	0.952

Note: Combined MRI: dynamic MRI + hepatobiliary phase MR images.

[†]There was a significant differences in Az values between dynamic MRI and combined MRI for both readers ($p < 0.0166$: $p = 0.0083$ for reader 1, $p = 0.0162$ for reader 2).

*There was a significant difference in Az values between MDCT and combined MRI for both readers ($P < 0.0166$: $p = 0.0027$ for reader 1, 0.0027 for reader 2).

There were no significant differences in Az values between MDCT and dynamic MRI for both readers.

the three sets of images (MDCT, dynamic MRI, and combined MRI) in the diagnosis of HCC for each reader. Areas under the empiric ROC curves (Az values) were estimated nonparametrically and compared between the three sets of images. Subsequently, sensitivity and specificity were calculated for each set of images. To that end, confidence scores of 1–3 were considered negative for HCC, whereas confidence scores of 4 and 5 were regarded as positive for HCC. Differences in sensitivity and specificity between the three sets of images were assessed using the McNemar test. All analyses were done for both observers separately. Reader agreement at MDCT, dynamic MRI, and combined MRI was analyzed using the weighted κ statistic, defined as poor (<0.2), fair (>0.2 to ≤ 0.4), moderate (>0.4 to ≤ 0.6), good (>0.6 to ≤ 0.8), and excellent (>0.8 to ≤ 1) agreement. $P < 0.0166$ was considered to indicate a statistically significant difference because we employed Bonferroni correction for comparing the results among the three groups. All analyses were performed using commercial statistical software (JMP, v. 8; SAS Institute Japan, Tokyo, Japan).

RESULTS

ROC Analysis

Az values for the diagnosis of HCC of each set of images for both readers are shown in Table 2. The two readers had comparable (not significantly different) Az values for all lesions between MDCT (0.921 for reader 1, and 0.917 for reader 2) and dynamic MRI (0.925 for reader 1, and 0.935 for reader 2). However, both readers achieved significantly higher Az values for all lesions with combined MRI (0.961 for reader 1, and 0.967 for reader 2) than with dynamic MRI ($P = 0.0083$ for reader 1, and $P = 0.0162$ for reader 2). In addition, for smaller lesions (<1.5 cm) the Az value with combined MRI was significantly higher than that with MDCT for both readers ($P = 0.0027$ for readers 1

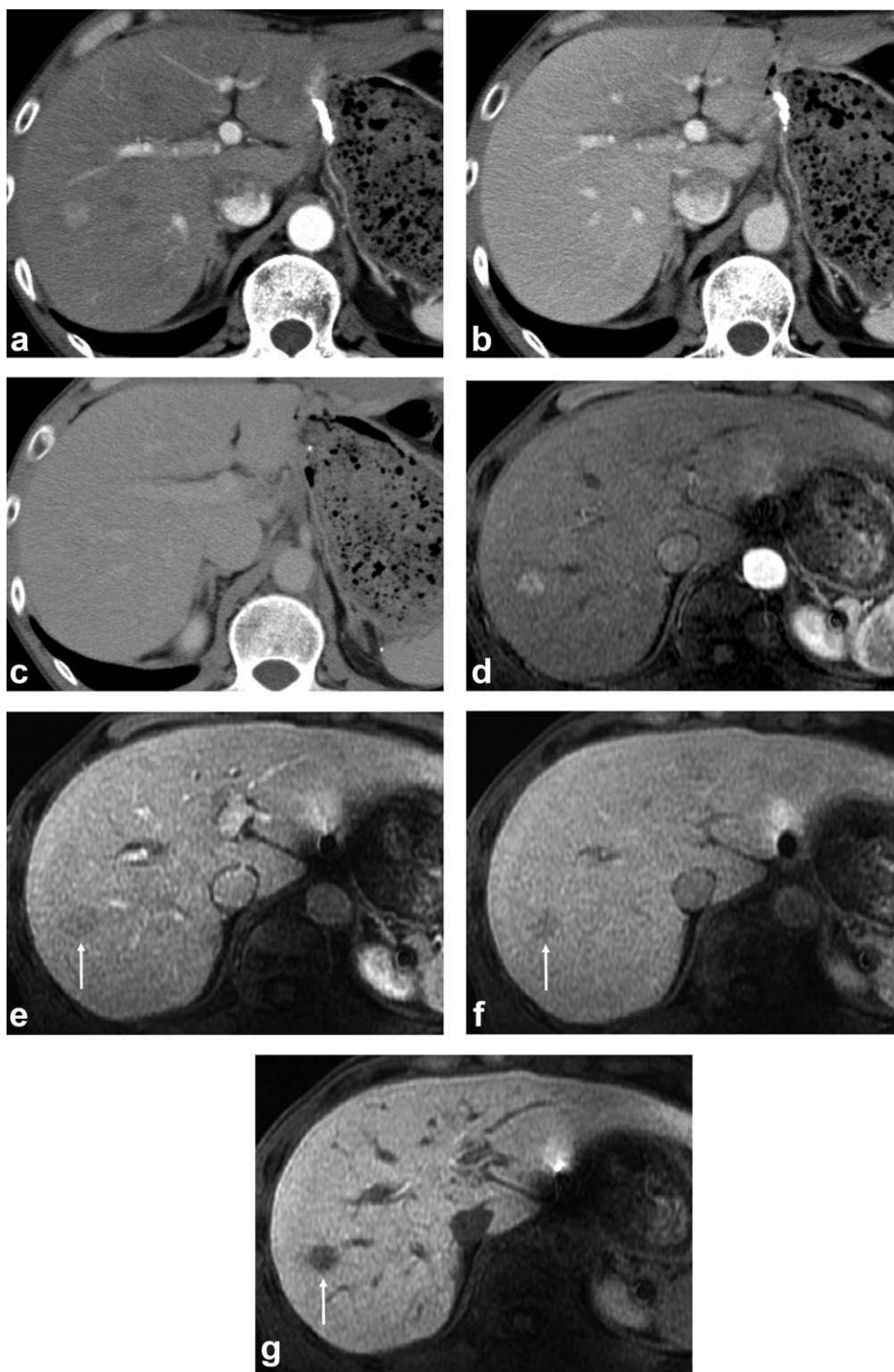


Figure 1. A 55-year-old man with a history of hepatitis C cirrhosis (Child-Pugh A) and biopsy-proven moderately differentiated HCC. **(a)** MDCT and **(d)** EOB-enhanced arterial phase MR image demonstrate a hypervascular nodule at segment VI-VII. In **(e,f)** EOB MR images obtained during portal venous and equilibrium/late phases, rapid washout (arrows) is seen, although this finding is unclear in **(b,c)** MDCT images obtained during portal venous and equilibrium phases. In **(g)** the Gd-EOB-enhanced hepatobiliary phase MR image at 20 minutes, the nodule is clearly hypointense (arrow) compared to surrounding liver parenchyma.

and 2) (Fig. 1). Reader agreement for the diagnosis of HCC using MDCT, dynamic MRI, and combined MRI was good to excellent, given the κ values of 0.921 (95% confidence interval [CI]: 0.881–0.961), 0.921 (95% CI: 0.882–0.960), and 0.789 (95% CI: 0.727–0.850), respectively.

Sensitivity and Specificity

Sensitivities and specificities of each set of images for both readers are shown in Table 3. The sensitivities

for all lesions increased with the additional interpretation of hepatobiliary phase images (combined MRI) from 75.0% to 86.7% and from 78.3% to 86.7% for readers 1 and 2, respectively, and the significant differences were achieved between it and MDCT ($P = 0.0045$ for reader 1, $P = 0.0126$ for reader 2) for both readers and were also observed between it and dynamic MRI ($P = 0.0082$ for reader 1. The sensitivities for smaller lesions (<1.5 cm) with combined MRI were significantly higher than those with MDCT ($P = 0.0143$ for reader 1, and $P = 0.0143$ for reader 2) for

Table 3
Sensitivity and specificity of each set of images in the diagnosis of HCC for each reader

	MDCT	Dynamic MRI	Combined MRI
All lesions (n = 60)			
Reader 1			
Sensitivity	68.3 (41/60)	75.0 (45/60)	86.7 (52/60)*,†
Specificity	94.9 (37/39)	92.3 (36/39)	89.7 (35/39)
Reader 2			
Sensitivity	71.7 (43/60)	78.3 (47/60)	86.7 (52/60)*
Specificity	94.9 (37/39)	94.9 (37/39)	92.3 (36/39)
Lesion <1.5 cm (n = 16)			
Reader 1			
Sensitivity	56.3 (9/16)	81.3 (13/16)	93.8 (15/16)*
Specificity	96.7 (29/30)	96.7 (29/30)	96.7 (29/30)
Reader 2			
Sensitivity	56.3 (9/16)	75.0 (12/16)	93.8 (15/16)*
Specificity	96.7 (29/30)	96.7 (29/30)	96.7 (29/30)

Note: Combined MRI: dynamic MRI + hepatobiliary phase MR images.

Data are percentages with numbers used to calculate percentages in parentheses.

*There was a significant difference in sensitivities between MDCT and combined MRI for both readers (All lesions: $p = 0.00045$ for reader 1, $p = 0.0126$ for reader 2; Lesion < 1.5 cm: $p = 0.0143$ for reader 1, $p = 0.0143$ for reader 2).

†There was a significant difference in sensitivities between dynamic MRI and combined MRI for reader 1 ($p = 0.0082$). Specificities between the three sets of images were not significantly different.

both readers, although there were no significant differences between dynamic MRI and combined MRI. Meanwhile, the specificities of all imaging modalities were higher (about 90%) without any significant differences among the three sets of images sets for both readers.

False-Negative Nodules

Among all HCCs, 53 (88.3%) HCCs were hypointense in the hepatobiliary phase, whereas five (8.3%) and two (3.3%) were hyperintense and isointense, respectively.

CT and MR findings of false-negative nodules with a score of 1 or 2 are summarized in Table 4. The number of false-negative nodules on MDCT for readers 1 and 2 were both 14, and those on dynamic MRI were 11 and 10, respectively. The majority of these nodules (75% and 62% for MDCT and dynamic MRI, respectively) were mischaracterized due to a lack of identification of washout findings, although arterial enhancement could be identified (Figs. 1, 2). Among these nodules, five nodules (45.5%, 5/11) for reader 1 and five (50.0%, 5/10) for reader 2 showed hypointensity to surrounding liver parenchyma during hepatobiliary phases (Fig. 2). On the other hand, four nodules became hyperintense to surrounding liver parenchyma during hepatobiliary phases because of uptake of the contrast into the HCC. Only one nodule which was missed with both dynamic and combined MRI was correctly judged as HCC on MDCT by both readers. Meanwhile, the two false-negative nodules, which did not show any arterial enhancement on both MDCT and dynamic MRI were hypointense ($n = 2$) during hepatobiliary phase images. The pathological examination proved that all these nodules were well-differentiated HCCs.

False-Positive Lesions

Both readers recorded one false-positive nodule for MDCT, two for dynamic MRI, and three for combined

MRI. The false-positive CT findings were attributed to A-P shunts (10 mm in size). The false-positive MR findings were attributable to one high-flow hemangioma and two A-P shunts, which showed hypointensity to surrounding liver parenchyma during equilibrium and hepatobiliary phases (Fig. 3).

DISCUSSION

The results of our study demonstrate that the accuracy of dynamic EOB-enhanced MRI for the diagnosis of early stage HCC is equivalent to that of MDCT,

Table 4

Characteristics of false negative nodules with a score of 1 and 2 on dynamic MDCT and MRI, and signal intensity on hepatobiliary phase images, for each reader

	MDCT	MRI Set 1	SI on HB phase
Reader 1	n = 14	n = 11	
A.E. (+)/Washout (–)	11(78.6)	7(63.6)	low 3 high 3 iso 1
A.E. (–)/Washout (+)	2 (14.3)	1 (9.1)	low 1
A.E. (–)/Washout (–)	1 (7.1)	3 (27.3)	low 1 high 1 iso 1
Reader 2	n = 14	n = 10	
A.E. (+)/Washout (–)	10 (71.4)	6 (60.0)	low 3 high 3 iso 0
A.E. (–)/Washout (+)	2 (14.3)	1 (10.0)	low 1
A.E. (–)/Washout (–)	2 (14.3) iso 1	3 (30.0)	low 1 high 2

Note: MRI Set 1: Dynamic MR images alone, MRI Set 2: Combined dynamic and hepatobiliary phase MR images.

Abbreviations: A.E., arterial enhancement; SI, signal intensity; HB, hepatobiliary phase. Data are absolute numbers with percentages in parentheses.

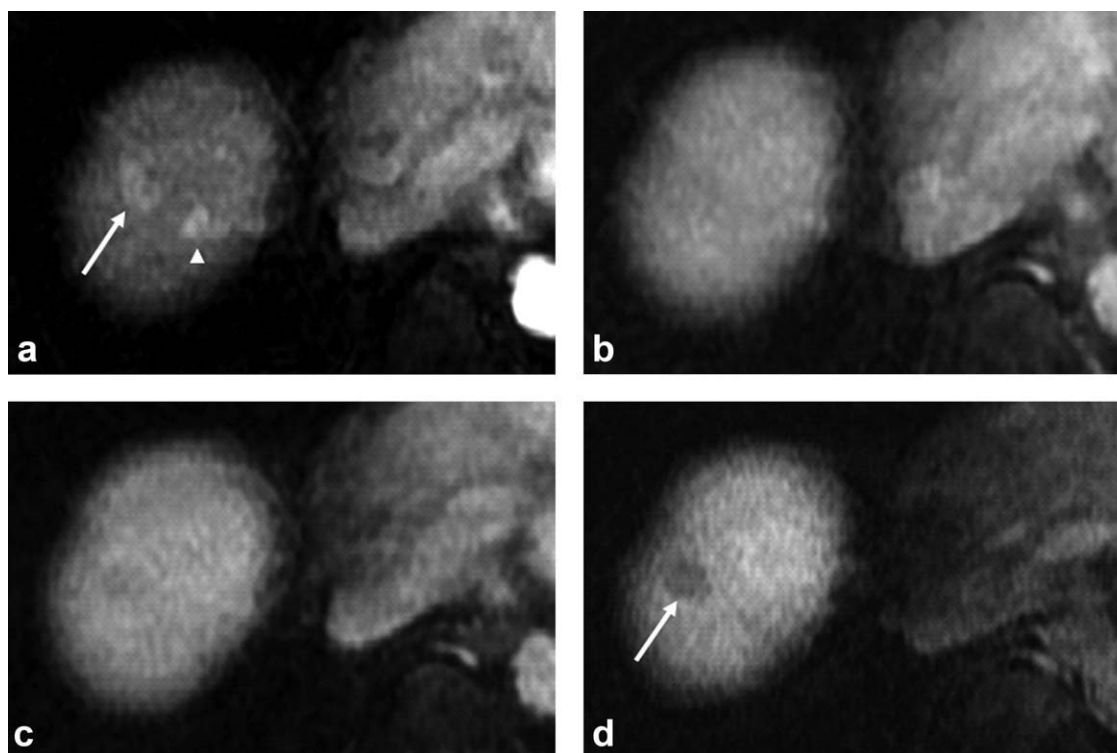


Figure 2. A 70-year-old man with a history of hepatitis C cirrhosis (Child-Pugh B) and biopsy-proven moderately differentiated HCC. Gd-EOB-enhanced arterial phase MR image shows a hypervascular nodule (arrow) at segment VIII (hepatic dome). Small A-P shunt (arrowhead) near the lesion is also seen on the Gd-EOB-enhanced arterial phase MR image. **b,c:** In Gd-EOB-enhanced portal venous and late phases MR images, the washout finding is unclear, with a score of 3 assigned by both readers. On the other hand, **(d)** the Gd-EOB-enhanced hepatobiliary phase MR image at 20 minutes clearly shows a hypointense nodule (arrow) at segment VIII (hepatic dome). Both readers judged this nodule as HCC (score of 5).

whereas the combined interpretation of dynamic and hepatobiliary phase images significantly improves sensitivity and accuracy for the diagnosis of lesions less than 1.5 cm in diameter, compared with either dynamic EOB-enhanced MRI or triple-phase dynamic MDCT.

Although the total amount of gadolinium of EOB (concentration; 0.25 mmol/mL, administration volume; 0.1 mL/kg) is one-quarter of that of other, standard gadolinium chelate agents (concentration; 0.5 mmol/mL, administration volume; 0.2 mL/kg), in this study we found comparable arterial phase results in hypervascular HCCs with Gd-EOB-DTPA and MDCT as previously reported (21,22). The number of missed HCC nodules ($n = 1$ for both readers) with dynamic EOB-enhanced MRI in the arterial phase was almost equal to that with MDCT ($n = 2$ for both readers). Compared to the T1 relaxivity of standard gadolinium chelate agents in blood (about $4.5 \text{ Lmmol}^{-1}\text{s}^{-1}$), the relaxivity of EOB ($8.2 \text{ Lmmol}^{-1}\text{s}^{-1}$) is increased in human blood by the extent of protein binding (10.7%), which is higher than that of standard gadolinium chelate agents (1.6%). Thus, its higher T1 relaxivity can compensate for the lower amount of gadolinium. In addition to the characteristic molecular action of EOB, other factors supporting the better results with EOB are essential. As described, the bolus administration volume with EOB is only half of standard gadolinium chelate

agents. Therefore, more exact scan timing for arterial phase imaging is needed to achieve the potential ability of EOB. We used the MR fluoroscopic bolus detection technique (CARE Bolus) for this purpose in this study. Additionally, we selected a relatively slow injection rate (1 mL/sec) to reduce artifacts and accelerate protein binding of EOB in human blood because a faster injection rate may induce signal inhomogeneities in k -space, causing ringing artifacts (20). The use of recently developed high-resolution 3D-GRE sequences with fat saturation (VIBE) also provides higher liver-lesion contrast, as researchers have described previously (23).

Thanks to recent advances in hardware, improvements in spatial resolution, and contrast injection methods, the sensitivities of dynamic MDCT and MRI with nonspecific extracellular agents for the diagnosis of HCC appear to have increased (24). However, the diagnosis of small HCC is still challenging because of variable vascular characteristics of HCCs. In the present study the majority of false-negative nodules on MDCT and dynamic EOB-enhanced MRI (75% and 62% for MDCT and dynamic MRI, respectively) were due to a lack of identification of washout findings, although arterial enhancement could be identified. The identification of washout findings in the portal venous or late phase is crucial for a reliable diagnosis of HCC, especially for the differentiation from nonneoplastic early arterial enhancement (focal A-P shunt).



Figure 3. A 67-year-old man with a history of chronic hepatitis C with focal A-P shunt. Gd-EOB-enhanced arterial phase MR image shows a hypervascular nodule (arrow) at segment VIII. In (b) the Gd-EOB-enhanced portal venous phase MR image, the nodule is isointense to surrounding liver parenchyma. In (c,d) Gd-EOB-enhanced late and hepatobiliary phases MR images at 20 minutes, the nodule (arrows) is faintly hypointense to surrounding liver parenchyma with a score of 4 assigned by both readers. Also note a hypointense tiny cyst (arrowhead) near this nodule at segment IV on the hepatobiliary phase image at 20 minutes. In (e) the T2-weighted image, the nodule is not visible.

Although the identification rate of arterial enhancement of the tumors on both MDCT and MRI is mainly influenced by the contrast injection and acquisition methods, that of the washout finding is mainly determined by the histopathological characteristics of HCCs, which are also linked to their tumor sizes.

As recent researchers reported, the MR images in the hepatobiliary phase with EOB contribute to improvement of tumor detection and characterization (10,13–18). Usually, the majority of hypervascular

HCCs appear hypointense (88.3% in this study) in the hepatobiliary phase due to lack of normal hepatocytes in the tumor (9,21). In present study, among all false-negative nodules on dynamic MRI, five nodules (45.5% for reader 1 and 50.0% for reader 2) showed hypointensity to surrounding liver parenchyma during the hepatobiliary phase, and this additional information could improve the diagnosis of HCC. Moreover, the sensitivity and accuracy for the diagnosis of lesions less than 1.5 cm in diameter with combined

MRI were also significantly higher than those of triple-phase dynamic MDCT. Therefore, added interpretations of hepatobiliary phase images could significantly improve the diagnosis of HCC, in particular in small lesions showing isointensity during portal venous or equilibrium phases, which could be difficult to differentiate from nonneoplastic early arterial enhancement (focal A-P shunt). Moreover, EOB-enhanced MRI may allow for the demonstration of minimal dedifferentiated hepatocytes within the tumors prior to changes of tumor vascularity.

Meanwhile, the diagnosis of HCCs showing paradoxical uptake of EOB, ie, those appearing isointense or hyperintense compared to surrounding liver parenchyma, may be problem. In the present study, 11.6% of 60 HCCs exhibited hyperintensity (8.3%) or isointensity (3.3%) compared to surrounding liver parenchyma on hepatobiliary phase images. Some investigators have indicated that some well- or moderately differentiated HCCs may exhibit hyperintensity or isointensity on hepatobiliary images, while some researchers and our experience indicate that cirrhosis-related benign nodules (eg, large regenerative or dysplastic nodules) may have the same signal on hepatobiliary phase images (25). Overlapping findings between HCC and cirrhosis-related benign nodules were observed, although lesions showing hyperintensity on T2WI or DWI may be suggested in the diagnosis of HCC. Further research is needed to determine confident imaging criteria for the diagnosis of these HCCs.

In this study, both readers recorded one false-positive nodule on MDCT, two on dynamic MRI, and three on combined MRI. The false-positive CT findings were attributed to A-P shunts. The false-positive MR findings were attributed to one high-flow hemangioma and two A-P shunts (Fig. 3). As previous investigators have indicated, high-flow hemangioma may show relative hypointensity compared to surrounding liver parenchyma during equilibrium or hepatobiliary phases, which is called the "pseudo washout" sign (26). The period in which EOB acts as an extracellular agent is shorter than other contrast agents and it is quite rapidly taken up in the normal functioning liver. Therefore, in some high-flow hemangiomas the characteristic prolonged enhancement might be diminished during equilibrium or hepatobiliary phases, which could thus mimic hypervascular HCCs. Nevertheless, the presence of high signal intensity on T2WI for hemangioma may be helpful for differentiating high-flow hemangiomas from hypervascular HCCs.

In line with previous reports, the remaining false-positive nodules on MDCT and Gd-EOB-DTPA enhanced MRI were attributed to A-P shunts (13). Although A-P shunts usually exhibit a signal intensity identical to that of surrounding liver parenchyma on Gd-EOB-DTPA-enhanced MRI, we found that two A-P shunts (7.69%, 2/26) showed hypointensity compared to surrounding liver parenchyma during equilibrium or hepatobiliary phases, as has also been reported in a recent study (27).

This study had some limitations. First, our study was retrospective. Further, prospective research is

needed to confirm our results. Second, we included a relatively large number of patients with good liver function, and the number of patients with advanced or endstage liver cirrhosis, in whom liver enhancement after EOB injection could be worse, was relatively low. This factor could affect our results, although it should be noted that the diagnosis of HCC in patients with maintained liver function has more important therapeutic implications than in those with a poor liver function. Finally, the benign lesions in this study included hemangiomas and A-P shunts. Although these benign liver lesions are common and their differentiation from hypervascular HCCs is an important diagnostic issue, no other types of benign liver lesions were included. Some cirrhotic benign nodules (eg, regenerative nodules, dysplastic nodules, or focal nodular hyperplastic areas) could have an atypical enhancement behavior during dynamic and hepatobiliary phases, mimicking HCCs. Further research including a wider spectrum of benign lesions is needed.

In conclusion, the performance of dynamic EOB-enhanced MRI for the diagnosis of early stage HCC is equivalent to that of triple-phase dynamic MDCT. The diagnostic performance of dynamic EOB-enhanced MRI can significantly be improved by adding hepatobiliary phase images, in particular in small lesions showing isointensity during portal or equilibrium phases. The sensitivity and accuracy of EOB-enhanced MRI with hepatobiliary phase imaging were significantly superior to MDCT for the diagnosis of lesions less than 1.5 cm in diameter. EOB-enhanced MRI has the potential to replace dynamic MDCT imaging and could become a promising modality for the noninvasive management of patients with HCC.

REFERENCES

1. Parkin DM, Bary F, Ferlay J, Pisani P. Global cancer statistics, 2002. *CA Cancer J Clin* 2005;55:74–108.
2. American Cancer Society. Cancer facts and figures 2005. Atlanta, GA: American Cancer Society; 2005.
3. Llovet JM, Brú C, Bruix J. Prognosis of hepatocellular carcinoma: the BCLC staging classification. *Semin Liver Dis* 1999;19:329–338.
4. Mazzaferro V, Regalia E, Doci R, et al. Liver transplantation for the treatment of small hepatocellular carcinomas in patients with cirrhosis. *N Engl J Med* 1996;14:693–699.
5. Freeman RB, Mithoefer A, Ruthazer R, et al. Optimizing staging for hepatocellular carcinoma before liver transplantation: a retrospective analysis of the UNOS/OPTN data base. *Liver Transpl* 2006;12:1504–1511.
6. Peterson MS, Baron RL, Marsh JW Jr, Oliver JH, 3rd, Confer SR, Hunt LE. Pretransplantation surveillance for possible hepatocellular carcinoma in patients with cirrhosis: epidemiology and CT-based tumor detection rate in 430 cases with surgical pathologic correlation. *Radiology* 2000;217:743–749.
7. Forner A, Vilana R, Ayuso C, et al. Diagnosis of hepatic nodules 20 mm or smaller in cirrhosis: prospective validation of non-invasive diagnostic criteria for hepatocellular carcinoma. *Hepatology* 2008;47:97–104.
8. Reimer P, Schneider G, Schima W. Hepatobiliary contrast agents for contrast-enhanced MRI of the liver: properties, clinical development and applications. *Eur Radiol* 2004;14:559–578.
9. Huppertz A, Haraida S, Kraus A, et al. Enhancement of focal liver lesions at gadoteric acid-enhanced MR imaging: correlation with histopathologic findings and spiral CT-initial observations. *Radiology* 2004;230:266–275.

10. Huppertz A, Balzer T, Blakeborough A, et al. Improved detection of focal liver lesions at MR imaging: multicenter comparison of gadoxetic acid-enhanced MR images with intraoperative findings. *Radiology* 2004;230:266–275.
11. Bruix J, Sherman M. Practical Guidelines Committee, American Association for the Study of Liver Disease management of hepatocellular carcinoma. *Hepatology* 2005;42:1208–1236.
12. Bruix J, Sherman M, Llovet JM, et al. EASL Panel Experts on HCC. Clinical management of hepatocellular carcinoma. Conclusions of the Barcelona-2000 EASL conference. *J Hepatol* 2001;35:421–430.
13. Kim SH, Kim SH, Lee J, et al. Gadaxetic acid-enhanced MRI versus triple-phase MDCT for the preoperative detection of hepatocellular carcinoma. *AJR Am J Roentgenol* 2009;192:1675–1681.
14. Di Martino M, Marin D, Guerrisi A, et al. Intraindividual comparison of gadoxetate disodium-enhanced MR imaging and 64-section multidetector CT in the Detection of hepatocellular carcinoma in patients with cirrhosis. *Radiology* 2010;256:806–816.
15. Akai H, Kiryu S, Matsuda I, et al. Detection of hepatocellular carcinoma by Gd-EOB-DTPA-enhanced liver MRI: comparison with triple phase 64 detector row helical CT. *Eur J Radiol* 2010 DOI: 10.1016/j.ejrad.2010.07.026.
16. Ahn SS, Kim MJ, Lim JS, et al. Added value of gadoxetic acid-enhanced hepatobiliary phase MR imaging in the diagnosis of hepatocellular carcinoma. *Radiology* 2010;255:459–466.
17. Mita K, Kim SR, Kudo M, et al. Diagnostic sensitivity of imaging modalities for hepatocellular carcinoma smaller than 2 cm. *World J Gastroenterol* 2010;16:4187–4192.
18. Ichikawa T, Saito K, Yoshioka N, et al. Detection and characterization of focal liver lesions: a Japanese phase III, multicenter comparison between gadoxetic acid disodium-enhanced magnetic resonance imaging and contrast-enhanced computed tomography predominantly in patients with hepatocellular carcinoma and chronic liver disease. *Invest Radiol* 2010;45:133–141.
19. World Medical Association Declaration of Helsinki: ethical principles for medical research involving human subjects. *IAMA* 2000;284:3043–3045.
20. Haradome H, Grazioli L, Tsunoo M, et al. Can MR fluoroscopic triggering technique and slow rate injection provide appropriate arterial phase images with reducing artifacts on gadoxetic acid-DTPA (Gd-EOB-DTPA)-enhanced hepatic MR imaging? *J Magn Reson Imaging* 2010;32:334–340.
21. Frericks BB, Loddenkemper C, Huppertz A, et al. Qualitative and quantitative evaluation of hepatocellular carcinoma and cirrhotic liver enhancement using Gd-EOB-DTPA. *AJR Am J Roentgenol* 2009;193:1053–1060.
22. Vogl TJ, Kummel S, Hammerstingl R, et al. Liver tumors: comparison of MR imaging with Gd-EOB-DTPA and Gd-DTPA. *Radiology* 1996;200:59–67.
23. Rofsky NM, Lee VS, Laub G, et al. Abdominal MR imaging with a volumetric interpolated breath-hold examination. *Radiology* 1999;212:876–884.
24. Zhao H, Yao JL, Wang Y, Zhou KR. Detection of small hepatocellular carcinoma: comparison of dynamic enhancement magnetic resonance imaging and multiphase multirow-detector helical CT scanning. *World J Gastroenterol* 2007;13:1252–1256.
25. Cruite I, Schroeder M, Merkle EM, Sirlin CB. Gadaxetate disodium-enhanced MRI of the liver: part 2, protocol optimization and lesion appearance in the cirrhotic liver. *AJR Am J Roentgenol* 2010;195:29–41.
26. Doo KW, Lee CH, Choi JW, et al. "Pseudo washout" sign in high-flow hepatic hemangioma on gadoxetic acid contrast-enhanced MRI mimicking hypervascular tumor. *AJR Am J Roentgenol* 2009;193:W490–496.
27. Motosugi U, Ichikawa T, Sou H, et al. Distinguishing hypervascular pseudolesions of the liver from hypervascular hepatocellular carcinomas with gadoxetic acid-enhanced MR imaging. *Radiology* 2010;256:151–158.